High-pressure neutron diffraction on fluid methane

G. Strauß,[1] A. Bassen,[1] H. Zweier,[1] H. Bertagnolli,[1] K. Tödheide,[2] A. K. Soper,[3] and J. Turner[3]
[1]*Institut für Physikalische Chemie, Universität Stuttgart, Pfaffenwaldring 55, D-70569 Stuttgart, Germany*
[2]*Institut für Physikalische Chemie, Universität Karlsruhe, Kaiserstraße 12, D-76131 Karlsruhe, Germany*
[3]*Rutherford Laboratory, Chilton, Didcot, Oxon OX11 0QX, United Kingdom*
(Received 7 August 1995)

High pressure neutron diffraction measurements of the structure factor of fluid methane (CD_4) at $T=370$ K and three supercritical densities are presented, and the intra- and intermolecular structures are determined. The variation of the density has only a weak effect on the intermolecular distribution functions. Statistical mechanical calculations according to the extended reference interaction site model formalism were performed, and an intermolecular potential of a (12-6) Lennard-Jones type with partial charges on the atoms was deduced that reproduces the experimental total atom correlation functions at all investigated thermodynamic states. Additionally, the corresponding structure factor of statistically orientated methane molecules was calculated. As the agreement between experiment and theory is very good, it is concluded that no orientational correlation exists in fluid methane. Reverse Monte Carlo calculations (RMC) were performed with the recently developed optimization algorithm great deluge [G. Dueck, J. Comput. Phys. **104**, 86 (1993)]. This is a non-Boltzmann sampling method specially used for minimizing the difference between the experimental and the simulated intermolecular distribution function. The results, obtained by RMC, confirm the statistical mechanical calculations and show that the distribution of the molecules in fluid methane is randomly distributed and no orientational correlation between the molecule axes exists.

PACS number(s): 61.12.−q, 61.20.−p

I. INTRODUCTION

As is well known, the chemical and physical properties of the alkanes change systematically with increasing chain length. In order to find a generally valid theory of the behavior of the alkanes, many experimental investigations and theoretical considerations were carried out on them. One of the first theories was proposed by Prigogine, Bellemans, and Mathot [1]. The theory is a generalization of the principle of corresponding states and is based on a cell model. Each molecule is subdivided into quasispherical segments whose interactions are characterized by the distance d and the energy ϵ. Since the molecule is described by a chain of spherical elements, no change of properties of the system should be expected in this model if the total number of segments remains unaltered. A similar but more refined model for the description of molecular, alkanelike liquids is the fused hard-sphere (FHS) model and its extension, the so-called bonded hard-sphere (BHS) model [2,3]. In the FHS theory, the molecules are represented by overlapping hard spheres that usually coincide with the individual atoms forming the molecules. In this approach the properties of polyatomic molecules are reduced to those of spheres. In the BHS theory the polyatomic molecules are modeled as tangentially bonded hard spheres, where spheres of type 1 make up the backbone of the chain and spheres of type 2 represent the substituent atoms. Good agreement between the BHS theory and Monte Carlo simulation, tested on thermodynamical properties of different alkanes, has been achieved [4–6], but the experimental verification is still lacking.

In principle, the experimental verification or falsification of statistical mechanical theories that start from an intermolecular potential can follow two routes. Thermodynamic data can be calculated by integration either of the intermolecular potential and the corresponding atom pair correlation function or of terms derived from both functions, over all distances. It is obvious that the integration of quite different functions can give almost the same results or, in other words, the reproduction of experimental thermodynamic values is a strong indication but not a proof of the validity of the applied potential. In comparison to that, a more stringent proof requires scattering experiments, as they give distance-dependent quantities, namely, the pair correlation functions.

According to our experience, data of at least three thermodynamic states are prerequisite to test the quality of intermolecular potentials and to detect trends in the intermolecular structure of liquids. As the structural changes are often small, measurements with high precision are required.

The simplest species in the homologous series of alkanes is methane. As methane is a spherical molecule, it serves as a model substance for theoretical studies. For example, methane was an object of many molecular dynamics calculations [7–16], Monte Carlo calculations [17], and experimental work [18–22] with the aim of deducing thermodynamic properties from microscopic properties. Despite the enormous theoretical interest, there exist few diffraction data with information on the microscopic structure of methane gas, i.e., the measurements of Habenschuss, Johnson, and Narten [23], who

performed x-ray diffraction on methane gas at its triple point, and the measurements of Johnson and Olsson [20], who investigated the translational and rotational motions of methane in a momentum range of $\kappa=0.8-2.0$ Å^{-1}. They concluded that it is necessary to extend the momentum range of the scattering functions and that they have to study the recoil effects first, because they found only weak temperature-dependent coupling effects, in contradiction to Habenschuss, Johnson, and Narten.

In view of the fundamental importance of the methane system for statistical mechanical theories and computer simulations, as well as for the need for a test of recent theories of the properties of alkanes, as described above, we performed neutron diffraction measurements of the structure factor of methane gas. As density-dependent measurements of the structure factor are a powerful tool for testing the quality of intermolecular potentials, which are prerequisite for describing structural properties of molecular liquids, the measurements were carried out at three supercritical thermodynamic states.

For all measured thermodynamic states we performed reverse Monte Carlo simulations and statistical mechanical calculations (the extended reference interaction side model), with the goal of deducing an intermolecular potential that describes the experimental data at all measured densities. Our intention was also to check the validity of the theories mentioned above or even to improve statistical mechanical theories on the basis of the experimental data. For instance, one question is whether we can reduce the characteristic features of the homologous series of the alkanes to the properties of the simplest representative of these organic compounds, methane. Another question is whether the methane molecule can be treated as a spherical molecule with a single Lennard-Jones potential and with only a spherical form factor needed to reproduce the neutron diffraction data. If the answer is yes, this would be a proof that no orientational correlation exists in fluid methane.

II. BASIC RELATIONS

The theory of neutron scattering by liquids is well described in the literature [24–27]. Therefore we give here only a short survey for a better understanding of the data evaluation in this work. The short-range order of a pure molecular liquid of number density ρ is described by a set of atom pair correlation functions $g_{\alpha\beta}(r)$, where the individual function $g_{\alpha\beta}(r)$ gives the relative probability to find an atom of type β at distance r from an atom of type α. The atom pair correlation functions are related to the partial structure factors $[S_{\alpha\beta}(\kappa)]$ in momentum space by Fourier transformation.

The sum of all atom pair correlation functions, weighted by the coherent scattering lengths of the corresponding atom pair, can be obtained by scattering experiments. The intensity of the fraction of the incident neutrons of the wavelength λ, scattered into an element of the solid angle $d\Omega$, is proportional to the differential scattering cross section $(d\sigma/d\Omega)$. In the case of elastic scattering, the scattering angle 2Θ and the wavelength λ are related to the momentum transfer κ by

$$\kappa=(4\pi/\lambda)\sin\Theta \ . \tag{1}$$

In the case of time-of-flight measurement, the wavelength λ of elastically scattered neutrons is given by

$$\lambda_e=\frac{2\pi\hbar t}{m_n(L_1+L_2)} \ , \tag{2}$$

where t is the time of flight, m_n the mass of the neutron, L_1 the flight path moderator to sample, and L_2 the flight path sample to detector. The differential scattering cross section consists of an incoherent and a coherent part. The latter is split into three terms

$$\left[\frac{d\sigma}{d\Omega}\right]=\left[\frac{d\sigma}{d\Omega}\right]_{\text{inc}}^{\text{self}}+\left[\frac{d\sigma}{d\Omega}\right]_{\text{coh}}^{\text{self}}+\left[\frac{d\sigma}{d\Omega}\right]_{\text{coh}}^{\text{intra}}+\left[\frac{d\sigma}{d\Omega}\right]_{\text{coh}}^{\text{inter}} \ . \tag{3}$$

The "self" term is the sum of the scattering of the isolated atoms of the molecule and is given by Eq. (4), where b_α stands for the coherent and incoherent scattering lengths of the atom α and the sum runs over all atoms of the molecule

$$\left[\frac{d\sigma}{d\Omega}\right]_{\text{coh}}^{\text{self}}+\left[\frac{d\sigma}{d\Omega}\right]_{\text{inc}}^{\text{self}}=\sum_{\alpha=1}^{m}(b_{\text{coh},\alpha}^2+b_{\text{inc},\alpha}^2) \ . \tag{4}$$

The remaining coherent part of the differential scattering cross section, called the distinct term $(d\sigma/d\Omega)_{\text{coh}}^{\text{dis}}$, contains the information about the intramolecular as well as the intermolecular structure of the liquid. The intermolecular term of the differential scattering cross section is related to the weighted sum of all intermolecular partial structure factors according to Eq. (5):

$$\left[\frac{d\sigma}{d\Omega}\right]_{\text{coh}}^{\text{inter}}=\rho\sum_{\alpha=1}^{m}\sum_{\beta=1}^{m}b_{\text{coh},\alpha}b_{\text{coh},\beta}S_{\alpha\beta}(\kappa) \ . \tag{5}$$

By Fourier transformation of the distinct term, the weighted sum of all atom pair correlation functions $G(r)$, denoted in the following as "total atom distribution function," is obtained:

$$G(r)=\sum_{\alpha=1}^{m}\sum_{\beta=1}^{m}\bar{b}_{\text{coh},\alpha}\bar{b}_{\text{coh},\beta}g_{\alpha\beta}(r) \ , \tag{6}$$

$$G(r)=1+\frac{1}{2\pi^2\rho\left[\sum_{\alpha=1}^{m}b_{\text{coh},\alpha}\right]^2}\times\int_0^{\kappa_{\max}}\left[\frac{d\sigma}{d\Omega}\right]_{\text{coh}}^{\text{dis}}j_0(\kappa r)\kappa^2 d\kappa \ , \tag{7}$$

$$\bar{b}_{\text{coh},\alpha}=\frac{b_{\text{coh},\alpha}}{\sum_{\alpha=1}^{m}b_{\text{coh},\alpha}} \ ; \tag{8}$$

$j_0(\kappa r)=\sin(\kappa r)/(\kappa r)$ is the spherical Bessel function of zeroth order [28].

If the molecular structure is known, the intramolecular

contribution can be calculated according to Eq. (9):

$$\left[\frac{d\sigma}{d\Omega}\right]_{\text{coh}}^{\text{intra}} = \sum_{\alpha=1}^{m} \sum_{\substack{\beta=1 \\ \beta\neq\alpha}}^{m} b_{\text{coh},\alpha} b_{\text{coh},\beta} j_0(\kappa r_{\alpha\beta}) e^{-n_{\alpha\beta}^2 \kappa^2/2} . \quad (9)$$

$r_{\alpha\beta}$ is the mean distance of the atoms α and β and $n_{\alpha\beta}$ the mean square amplitude of the displacement in direction of $\mathbf{r}_{\alpha\beta}$ [24,29].

The thermodynamic limit $\kappa \rightarrow 0$ of the total coherent differential cross section is related to the isothermic compressibility χ_T according to Eq. (10). This relation can be used to extrapolate $(d\sigma/d\Omega)_{\text{coh}}$ to small κ values that are not accessible by standard diffraction experiments

$$\lim_{\kappa\rightarrow 0}\left[\frac{d\sigma}{d\Omega}\right]_{\text{coh}} = \rho \chi_T k_B T \left[\sum_{\alpha=1}^{m} b_{\text{coh},\alpha}\right]^2 , \quad (10)$$

where k_B is the Boltzmann constant.

In a case of spherical symmetry, the intermolecular structure factor is described by a molecular center structure factor $S_{cc}(\kappa)$, which is the Fourier transform of the center-center correlation function [30]

$$(d\sigma/d\Omega)_{\text{coh}}^{\text{inter}} = \rho f_m^2(\kappa) S_{cc}(\kappa) \quad (11)$$

and $f_m(\kappa)$ is the so-called spherical form factor, which depends only on the scattering lengths of the atoms of the molecule and of the intramolecular distances r_α and assumes that the orientation of neighboring molecules is uncorrelated. For methane the center-center correlation function is identical to the carbon-carbon correlation function and the molecule form factor is explicitly given by

$$f_m(\kappa) = \sum_{\alpha=1}^{5} b_\alpha \frac{\sin(\kappa r_\alpha)}{\kappa r_\alpha} = b_{\text{C}} + 4 b_{\text{D}} \frac{\sin(\kappa r_{\text{CD}})}{\kappa r_{\text{CD}}} , \quad (12)$$

where r_{CD} is the distance between the molecule center, the carbon atom, and the hydrogen atoms.

III. EXPERIMENT

The high-pressure time-of-flight measurements on CD_4 were performed at SANDALS diffractometer at the ISIS pulsed neutron source (Rutherford Appleton Laboratory, Chilton, Didcot, United Kingdom). The CD_4 sample was purchased from MSD-Isotopes (MD-114) with an isotopic purity of 99.9%. The high-pressure cell was designed to withstand a pressure up to 1000 bar and consists of a cylinder with an outer diameter of 11.67 mm and an inner diameter of 7.6 mm, made of Ti-Zr zero alloy [31]. The top and bottom of the pressure cell were heated to prevent temperature drift. The pressure apparatus is described in detail in a previous paper [32]. Some modifications were made so that the thermodynamic variables pressure and temperature could be adjusted from outside the vacuum chamber. The geometrical setup remains unaltered throughout the course of the measurements, even for the measurements of the empty cell, since the pressure cell can be evacuated from outside. The scattered intensities of background, vanadium, filled container (with sample or with a vanadium rod inside), and empty container were recorded as a function of the neutron time of flight at ten scattering angles with zinc sulphide detectors. These detectors were 10 mm wide, 20 mm deep, and 200 mm tall, covering a scattering angle range of 3°–21° in a continuous range [33]. The incident wavelength range of the neutron beam was 0.05–4.0 Å with a beam of circular cross section and 32.0 mm in diameter.

It is a characteristic feature of high-pressure experiments that the signal-to-noise ratio, i.e., the difference between scattered intensities of the cell, filled with the sample, and the empty cell, is rather small. In order to obtain a satisfactory signal-to-noise ratio and to keep statistical error of each measurement constant as well as to check the reproducibility of the measurements, a set of four runs at the highest density and six runs at the lowest density were averaged, with a typical run lasting about 3 h at the normal ISIS proton current of 180 μA.

The measurements of the structure factor of CD_4 were performed at three thermodynamic states, given in Table I, with the PVT data taken from Ref. [18]. As the critical constants of CD_4 are $T_c = 190.8$ K, $p_c = 46.3$ bar, and $\rho_c = 0.164$ g cm^{-3} [18], all thermodynamic states studied were supercritical. During the measurements the fluctuations of pressure and temperature were within 0.4% and 0.3%, respectively.

IV. DATA EVALUATION

In order to evaluate the data, the energy scale was converted to neutron wave-vector change κ. The data were corrected for background, self-absorption, multiple scattering and normalized according to the ATLAS manual and with the procedures provided by the neutron facility of the Rutherford Appleton Laboratory [34]. The results of these corrections are the differential scattering cross sections for each scattering angle separately. Additionally, as already mentioned, we had measured a vanadium rod inside the pressure cell and evaluated the data like a sample to check the correction procedures with respect to the background, self-absorption, and multiple scattering of the high-pressure apparatus and the thick-walled pressure cell. By comparing the scattering intensities of the vanadium rod inside the pressure cell with the well defined theoretical intensities of vanadium, we detected small discrepancies in the normalization and corrected for it by using the data from a vanadium rod

TABLE I. Temperature, pressure, and density characterizing the thermodynamic states of the neutron diffraction experiments on supercritical CD_4 [18].

Temperature (K)	p (bar)	ρ (g cm^{-3})
370	510	0.27
370	610	0.31
370	770	0.34

TABLE II. Values for the calculated and the differential cross section extrapolated scattering intensities at $\kappa=0$ for the corresponding densities and isothermal compressibilities of CD_4. The PVT data for the calculation of χ_T are taken from Ref. [18].

$(d\sigma/d\Omega)_{coh}^{calc}$ (10^{-30} m^2)	$(d\sigma/d\Omega)_{coh}^{extrapol}$ (10^{-30} m^2)	ρ (g cm^{-3})	χ_T (10^{-8} m^2 N^{-1})
500	700	0.27	1.05
400	500	0.31	0.78
315	350	0.34	0.55

inside the pressure cell and its theoretical scattering for calibration of the samples.

As the neutrons are recorded at small angles at the instrument SANDALS, the inelasticity corrections are expected to be small. Nevertheless, the inelasticity effects become important for samples containing H atoms, especially in the region of $\kappa\rightarrow 0$.

Since the effect of inelastic scattering is not generally taken into account in the standard analytical correction procedures [35], we evaluated a procedure for the corrections that is based on an equation of Egelstaff [26], who has developed the formalism of Placzek [36] and Powles [37–42]. The inelastic correction is a function of Θ and κ, with the temperature, the effective mass of the sample, the scattering geometry, and the efficiency of the neutron detection process as parameters

$$P(2\Theta,\kappa_e)=-\frac{2ym_n}{M_{\text{eff}}}\left[\frac{aA+a+2}{a+1}\right]+\frac{m_n k_B T}{M_{\text{eff}}2E_0}\left[1-2y+\frac{4y(Aa+3)}{a+1}-\frac{2y[a^2B-6a(A+1)-3(5a-1)]}{(a+1)^2}\right], \tag{13}$$

where $y=\sin^2\Theta$, $\kappa_0=\kappa_e/2\sin\Theta$, $a=L_1/L_2$, $A=1-(\epsilon/\kappa_0)[1/E_d(\kappa_0)-1]$, $B=A+(\epsilon/\kappa_0)^2[1/E_d(\kappa_0)-1]$, $E_d(\kappa_0)=1-e^{-\epsilon/\kappa_e}$, $E_0=\hbar^2\kappa_0^2/2m$, m_n is the neutron mass, k_B is the Boltzmann constant, E_0 is the energy of the incoming neutrons, L_1 is the flight path of the incoming neutrons, L_2 is the flight path of the scattered neutrons, ϵ is the detector constant, M_{eff} is the effective mass of the sample, and T is the temperature of the sample. The important part of the program we used is based on a fit of the effective mass, in a κ range where the experimental intensities are oscillating about the single atom scattering. The value for the effective mass of the methane molecule at the investigated thermodynamic states, obtained from the best fit, is 7.4 g/mol. The Plazcek correction term is subtracted from the data according to

$$\left[\frac{d\sigma}{d\Omega}\right]^{\text{corrected}}=\left[\frac{d\sigma}{d\Omega}\right]^{\text{experimental}}-\left[\frac{d\sigma}{d\Omega}\right]^{\text{Plazcek}}. \tag{14}$$

Then we merged the data of the different scattering angles, taking into account only the region of overlapping.

In the experimentally inaccessible range of $\kappa\leq 0.35$ Å^{-1} the data were extrapolated to $\kappa=0$ Å^{-1} after having fitted the polynomial

$$(d\sigma/d\Omega)=a+b\kappa+c\kappa^2 \tag{15}$$

in the κ range of 0.35 Å$^{-1}\leq\kappa\leq 0.75$ Å^{-1}. The extrapolated scattering intensities $\lim_{\kappa\rightarrow 0}(d\sigma/d\Omega)_{coh}$ and the values calculated from the isothermic compressibility of CD_4 are given in Table II.

The discrepancy of extrapolated and calculated values of $(d\sigma/d\Omega)_{coh}$ at lower densities is caused by the behavior of χ_T. As χ_T diverges near the critical point, this tendency becomes apparent with decreasing density, which is closer to the critical one. The data evaluation was completed by the correction for systematic errors, a procedure first applied by Weidner, Geisenfelder, and Zimmermann [43]. In this procedure errors of the differential scattering cross section in the form of large periodic oscillations of usually low amplitude are corrected. The method corresponds to a low pass Fourier filter technique and is described in some detail in Ref. [32]. The resulting fully corrected coherent differential neutron scattering cross sections of methane at all thermodynamic states are given in Fig. 1. The determination of the molecular structure was performed iteratively by fitting the distinct term in a κ range where no (or only minor) intermolecular scattering contributes to the total scattering.

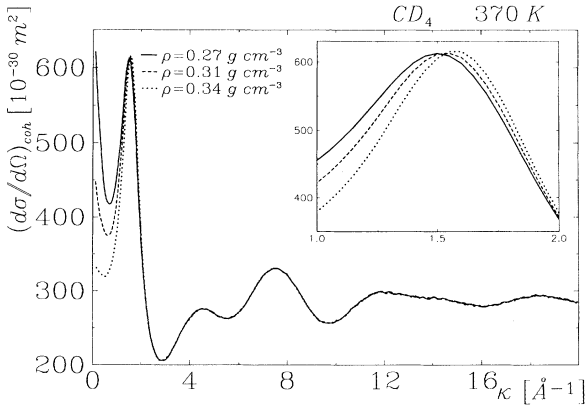

FIG. 1. Fully corrected coherent differential neutron scattering cross sections of CD_4 at 370 K and densities given in the legend.

TABLE III. Intramolecular distance C-D and Debye-Waller factors of CD_4, determined by fitting the distinct term of the structure factor at the different investigated thermodynamic states.

d_{CD}^{intra} (Å)	n_{CD} (Å)	n_{DD} (Å)	ρ (g cm^{-3})
1.099	0.0965	0.1407	0.27
1.099	0.0938	0.1422	0.31
1.099	0.0948	0.1423	0.34

V. RESULTS

The distinct term $(d\sigma/d\Omega)_{coh}^{dis}$ is split into the intermolecular part $(d\sigma/d\Omega)_{coh}^{inter}$ and the intramolecular part $(d\sigma/d\Omega)_{coh}^{intra}$; the corresponding Fourier transformations are denoted $G(r)^{inter}$ and $G(r)^{intra}$ in the following. The weighted sum of the total atom distribution function, defined by Eq. (6), is given in the case of CD_4 explicitly by

$$G(r)=0.040g_{CC}(r)+0.319g_{CD}(r)+0.641g_{DD}(r)\ . \quad (16)$$

A. Intramolecular structure

For the determination of the intramolecular part of $(d\sigma/d\Omega)$ it can be concluded from an approximately calculated intramolecular scattering intensity that the intermolecular contribution can be neglected at $\kappa \geq 5.0$ Å^{-1}. Therefore, an iterative fit, based on a Levenberg-Marquardt routine and taken from Ref. [44], was performed in that range. Owing to the high symmetry of the CD_4 molecule only one distance, namely, the C-D bond length, is sufficient for the calculations of all the other intramolecular distances and therefore only three parameters had to be fitted, namely, the intramolecular CD distance (r_{CD}^{intra}) and the Debye-Waller factors (n_{CD} and n_{DD}). The results of the fits are given in Table III and an example for the comparison of the fit with the experiment is shown in Figs. 2 and 3. In these figures the theoretically calculated molecular differential cross section of CD_4 and its Fourier transform, together with the corresponding experimental function for the fluid density $\rho=0.34$ g cm^{-3}, are shown. In view of the fact that only three

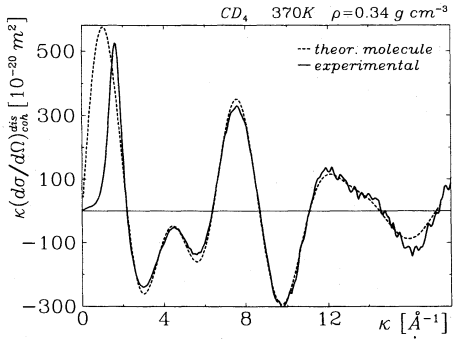

FIG. 2. Experimentally determined distinct term of CD_4 at 370 K, $\rho=0.34$ g cm^{-3}, and optimized theoretical intramolecular cross section.

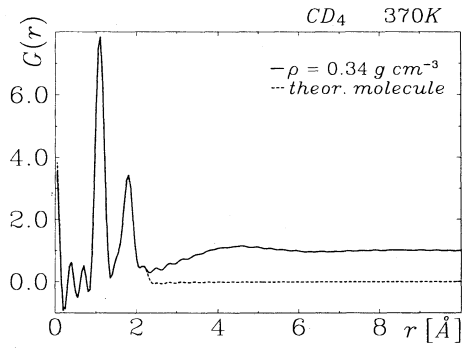

FIG. 3. Total atom pair correlation function of CD_4 at 370 K ($\rho=0.34$ g cm^{-3}) and the optimized theoretical intramolecular distribution function $G^{intra}(r)$.

parameters are sufficient for the calculation of the intramolecular part, the agreement of the experiment with the calculated $G(r)^{intra}$ function is excellent. The peak at $r \approx 1.1$ Å corresponds to the C-D bond length and at $r \approx 1.8$ Å to the *D-D* distance. The measured data (Fig. 1) were transformed in a κ range of 0.05 Å$^{-1} \leq \kappa \leq 17.9$ Å^{-1}. In Fig. 3 the maxima in $G(r)$ at values lower than $r=0.8$ Å are caused by termination-of-series errors of the Fourier transformation.

There exist two possibilities for determining the intramolecular structure. In general, if the largest intramolecular distances are on the order of the magnitude of the shortest intermolecular ones, it is quite difficult to separate them by means of Fourier transformation in a limited interval. But in our case, owing to the high symmetry of the molecule, the molecular geometry can be determined from the well defined first peak of the total atom distribution function that corresponds to the C-D bond length only. As we obtained nearly the same intramolecular distances for liquid and fluid densities of CD_4 (see Tables III and IV), we assume that the intramolecular geometry of CD_4 is not sensitive to density changes in the investigated pressure range.

B. Intermolecular structure

The goal of this work is to study the changes of the intermolecular distribution functions as the density is varied and to deduce an intermolecular potential that describes these changes in the range of investigated thermodynamic states. The intermolecular differential cross sec-

TABLE IV. Intramolecular distance C-D found in literature and determined in this work.

d_{CD}^{intra} (Å)	Reference
1.091 81	[63]
1.092	[64]
1.102	[65]
1.096	[66]
1.09	[16]
1.099	this work

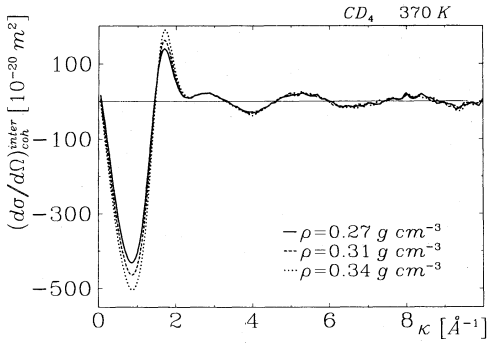

FIG. 4. Intermolecular part of the experimental differential scattering cross section of CD_4 at 370 K and specified densities.

tions of all measured thermodynamic states are given in Fig. 4. For a better comparison of the intermolecular distribution functions the corresponding intermolecular differential cross section of each thermodynamic state was Fourier transformed within the same κ range of about 0.05–10.0 $Å^{-1}$, where the exact upper limit was given by the zero transition of the $\kappa(d\sigma/d\Omega)^{\text{inter}}_{\text{coh}}$ function. A transformation to a higher κ value would improve the resolution in the distribution function, but would simultaneously increase the statistical uncertainty due to the noise in the reduced intensity, which increases with higher values of κ. The intermolecular distribution functions of all investigated thermodynamic states are given in Fig. 5.

Looking at Fig. 5 we see only one broad intermolecular peak at about 4.6 Å and a small shoulder at about 2.8 Å. So the intermolecular C-C, C-D, and D-D distances are not resolved in the $G(r)^{\text{inter}}$ function. The effects of the density change are only visible for a decrease of the minimum at 6.5 Å and a small shift of the maximum at 4.6 Å. This maximum corresponds to a superposition of all intermolecular distances. The density dependence of $G(r)$ is here only weak. Likewise the peak at $r=4.6$ Å becomes smaller with increasing density and is shifted to smaller-r values. This becomes more pronounced with increasing density, indicating an increase of the ordered

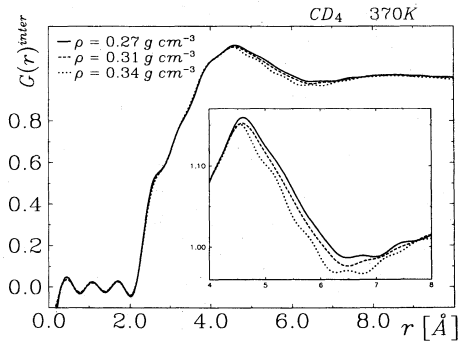

FIG. 5. Intermolecular total atom distribution functions of CD_4 at 370 K and specified densities given in legend.

state. At r values beyond about 8 Å the $G(r)$ functions approach the value 1, which corresponds to statistical disorder.

A detailed discussion of the individual site-site intermolecular radial distribution functions is not possible from the data alone, because the data represent only a weighted sum of correlations. Instead it is necessary to compare the data with the theoretically calculated functions. This will be done in the next section.

VI. REFERENCE INTERACTION SITE MODEL

The reference interaction site model (RISM) theory allows the atom pair correlation functions to be calculated from intermolecular atom pair potentials $u_{\alpha\beta}(r)$. The extended RISM (XRISM) theory expands the RISM theory to systems with long range interactions in the intermolecular potentials. It is common to both theories that they offer a powerful tool to check various potentials by comparing the results with those obtained by the experiments. The XRISM theory is already described in various publications [45–49] and so we only present here a brief summary of the required formalism.

The interaction-site model takes into account that each molecule is presented by interaction sites and the molecular potential is given by the sum of atom pair interactions $u_{\alpha\beta}(r)$. Usually hard-sphere or Lennard-Jones potentials are assumed, but a realistic potential must take into account the long-range interaction and therefore point charges are placed on the sites, the interactions of which are given by Coulomb potentials

$$u_{\alpha\beta}(r)=4\epsilon_{\alpha\beta}\left[\left[\frac{\sigma_{\alpha\beta}}{r_{\alpha\beta}}\right]^{12}-\left[\frac{\sigma_{\alpha\beta}}{r_{\alpha\beta}}\right]^{6}\right]+\frac{q_\alpha q_\beta}{4\pi\epsilon_0 r_{\alpha\beta}} . \quad (17)$$

The atom pair correlation is split into the direct correlation function $[c_{\alpha\beta}(r)]$ and the background function $[y_{\alpha\beta}(r)]$

$$h_{\alpha\beta}(r)=c_{\alpha\beta}(r)+y_{\alpha\beta}(r) . \quad (18)$$

The direct correlation function is related to $h_{\alpha\beta}(r)$ according to

$$h_{\alpha\beta}(r)=\sum_\gamma\sum_\delta \omega_{\alpha\gamma}(r)\circ c_{\gamma\delta}(r)\circ\omega_{\delta\beta}(r) + \sum_\gamma\sum_\delta \rho\omega_{\alpha\gamma}(r)\circ c_{\gamma\delta}(r)\circ h_{\delta\beta}(r) , \quad (19)$$

$$\omega_{\alpha\beta}(\kappa)=\delta_{\alpha\beta}+(1-\delta_{\alpha\beta})\frac{\sin(\kappa r)}{\kappa r} , \quad (20)$$

where $h_{\alpha\beta}(r)=g_{\alpha\beta}(r)-1$ and the circles symbolize the mathematical procedure of convolution. The correlation functions are given in matrix form

$$\hat{h}(r)=\hat{\omega}(r)\circ\hat{c}(r)\circ\hat{\omega}(r)+\rho\hat{\omega}(r)\circ\hat{c}(r)\circ\hat{\omega}(r) , \quad (21)$$

which is converted into a simple product by Fourier transformation

$$\hat{h}(\kappa)=\hat{\omega}(\kappa)\hat{c}(\kappa)\hat{\omega}(\kappa)+\rho\hat{\omega}(\kappa)\hat{c}(\kappa)\hat{\omega}(\kappa) . \quad (22)$$

The relation of $c_{\alpha\beta}(r)$ with the pair potential $u_{\alpha\beta}(r)$ and

TABLE V. Parameters of different (12-6) Lennard-Jones potentials according to Eq. (17) for methane (CD_4), deduced by Williams [52] and deduced in this work, where $Q_{AB}=1389.2 q_\alpha q_\beta$ kJ mol^{-1}, $q_\alpha=0.266$, and $q_\beta=-0.0665$.

AB	ϵ_{AB} (kJ mol^{-1})	σ_{AB} (Å)	Q_{AB} (kJ Å mol^{-1})	Reference
CC	0.40	3.25		[52]
CD	0.17	2.80		[52]
DD	0.06	2.42		[52]
CC	0.60	2.60	98.29	this work
CD	0.23	2.70	−24.57	this work
DD	0.09	2.80	6.143	this work

the background function $y_{\alpha\beta}(r)$ is given by various closures as the Percus-Yevick (PY) approximation [50]

$$c_{\alpha\beta}(r)=(e^{-u_{\alpha\beta}(r)/k_B T}-1)[y_{\alpha\beta}(r)+1] \quad (23)$$

or the hypernetted-chain (HNC) approximation [51]

$$c_{\alpha\beta}(r)=e^{-[u_{\alpha\beta}(r)/k_B T-y_{\alpha\beta}(r)]}-y_{\alpha\beta}(r)-1 \; . \quad (24)$$

As follows from these formulas, the intermolecular atom pair potential must be known in order to calculate the atom pair correlation function. We performed XRISM calculations on CD_4 for the thermodynamic states that were investigated and tested the PY and HNC approximations, assuming an intramolecular structure, listed in Table III. We checked the potentials for methane, given in literature [11,13,15,21,22,52,53], for our range of investigated thermodynamic states and found that the potential of Williams [52] reproduces our experimental data best. Habenschuss, Johnson, and Narten [23] also concluded by comparison with molecular dynamics calculations for methane, that the potential of Williams fits their results best. With the XRISM results of the potential of Williams (for the parameters see Table V) we could reproduce our experimental data qualitatively, but not the effects of density change. Therefore we added a Coulomb term and modified the values of the ϵ and σ parameters in such a way that we achieved better agreement between experiment and calculation. Often we succeeded in reproducing the experimental results for one thermodynamic state very well, but if we calculated the atom pair correlation functions of a different thermodynamic state, the results did not fit the experiment in a sufficient manner.

Therefore the criterion that a potential should be applicable for the complete range of thermodynamic states serves as a good check on the quality of a potential. The parameters of the potential we deduced from XRISM calculations are given in Table V. This potential, in combination with the HNC closure, reproduces the experimental results in the investigated range of thermodynamic states quite well, as shown in Fig. 6 together with the results of the potential of Williams. In this figure it can be seen that with decreasing density, particularly in the region of $r\approx 5$ Å, the results of the Williams potential differ more and more from the experimental data. The results of the potential deduced in this work, however, fit the experimental data of all investigated thermodynamic states well, particularly in the region of $r\approx 5$ Å, where the effects of the density change appear.

Since we found that the HNC approximation fits the experiments best, we show the dependence of density of the individual atom pair correlation functions, obtained with XRISM calculations and HNC closure, in Fig. 7. It is a characteristic of the observed peaks that the right-hand side of each main peak is broadened to larger-r values and the maxima of the peaks in the range 4–7 Å are reduced with increasing density. The effects are the same in all individual atom pair correlation functions. It should be mentioned that we cannot reproduce the $G(r)^{\text{inter}}$ functions exactly with the XRISM theory in the range of $r\leq 4.5$ Å, maybe owing to the approximate closure relations, and also the small-r region of the experimental functions are effected by truncation ripples, but we reproduced the small effect of the density changes in the region of $r\geq 4.5$ Å very well. The fit of a Gaussian function to the first peak of the center-center correlation function of $g_{cc}(r)$ gives coordination numbers from 4.5 at $\rho=0.27$ g cm^{-3} to 5.5 at $\rho=0.34$ g cm^{-3} and indicates, as can already be concluded from the shape of the curves, that the intermolecular short-range order is reduced with decreasing density.

VII. REVERSE MONTE CARLO SIMULATIONS

A. Method

Another method of interpreting diffraction data is provided by the reverse Monte Carlo simulation. This computer simulation method was developed by McGreevy and Pusztai [54] for structure modeling of amorphous systems without any assumption with respect to the intermolecular potentials. In contrast to other structure determination methods such as RISM, the reverse Monte

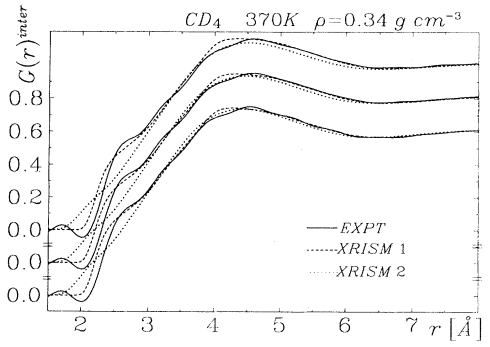

FIG. 6. Comparison of the weighted sums of intermolecular atom distribution functions of CD_4 at different thermodynamic states (from top to bottom $\rho=0.27$, 0.31, and 0.34 g cm^{-3}), obtained experimentally (EXPT) and by XRISM calculations (XRISM1, results of the potential deduced in this work; XRISM2, results of the potential deduced by Williams) with HNC closure (for the parameters of the potentials used, see Table V).

Carlo (RMC) simulation procedure directly generates a three-dimensional configuration that can be used for any kind of structural analysis, especially for studying the orientational relations of the molecules. In recent years the RMC method was already successfully applied to several atomic and molecular liquids and liquid mixtures [55–57]. As the method has been described in detail in these previous works, here we only give a brief summary of the basic principles, with a description of the latest development concerning approaches for accepting trial configurations in order to generate the final one.

The model system consists of a sphere and a surrounding shell of the thickness R_{max}. At the beginning of the simulation procedure the molecules are distributed randomly in the system with the correct experimental density. In this initial configuration the positions of the molecules as well as their orientational correlation are completely disordered and the closest intermolecular atom-atom distances are limited by cutoff-distances r_c, given for each atom pair. Now the molecules gradually move and rotate at random (up to maximum allowed values) in order to find a new configuration, the total atom pair correlation function $G_{calc}(r)$ of which is consistent with the experimental $G_{expt}(r)$ function. Therefore, $G_{calc}(r)$ is calculated after each move by summarizing the calculated atom pair correlation functions according to their neutron weighting factors. If the molecules do not overlap, as indicated by an atom-atom distance below the corresponding value of r_g (which is defined for each atom pair), the trial configuration is accepted for the moment with these parameters. Otherwise it is accepted with a probability according to a Gaussian distribution maximum at r_g and width σ_g. But the final decision on the acceptance depends on the deviation of the theoretical and the experimental distribution functions in the form of the χ^2 value

$$\chi^2=\sum_{i=1}^{i_{max}}\frac{[G_{expt}(r_i)-G_{calc}(r_i)]^2}{\sigma^2_{expt}}\ , \tag{25}$$

where i_{max} is the number of points in r space and σ^2_{expt} is the estimated error of the experiment. Whereas a decrease of the χ^2 value means an improvement of the fit and therefore the new generated configuration is accepted, an increase is only accepted with a Gaussian probability depending on the amount of the worsening. This algorithm, called simulated annealing, works well [57] and makes it possible to achieve a significantly better fit compared to an algorithm that strictly excludes worsening of the fit and where the system easily falls into a local minimum. The simulation is finished when χ^2 converges at a minimum value.

In this paper, we employed two recently developed optimization methods, the threshold accepting (TA) algorithm [58,59] and the great deluge (GD) algorithm [59,60] in order to test their suitability for achieving further improvements in the fit procedure by efficiently surmounting local minima. The TA algorithm is based on the following principles: Every new configuration is accepted provided that the new χ^2 value is not less than χ^2_{max}, which is the old χ^2 value plus a variable, called *threshold*. Over the course of the simulation, χ^2 mostly decreases, but with occasional increases, while the difference between χ^2 and χ^2_{max} remains constant. The use of the TA algorithm results in an oscillation of χ^2 around an average value after several simulation steps, which means that the simulation has reached a temporary convergence. Therefore, in regular steps (each n_{evt} moves) a check of the fit tendency is performed. If χ^2 lies below the value, reached at the last check, the threshold is kept constant. Otherwise, it is reduced by a defined percentage. In this way, the value of threshold falls over the course of the simulation, very quickly at the beginning and rather slowly at the end. The final convergence is reached when the further reduction of threshold does not reduce the value of χ^2. The implementation of this algorithm in the RMC program requires three parameters to be defined at the beginning of a simulation run: the initial value of the threshold, the number of steps (n_{evt}) between two checks of the trend of the fit, and the

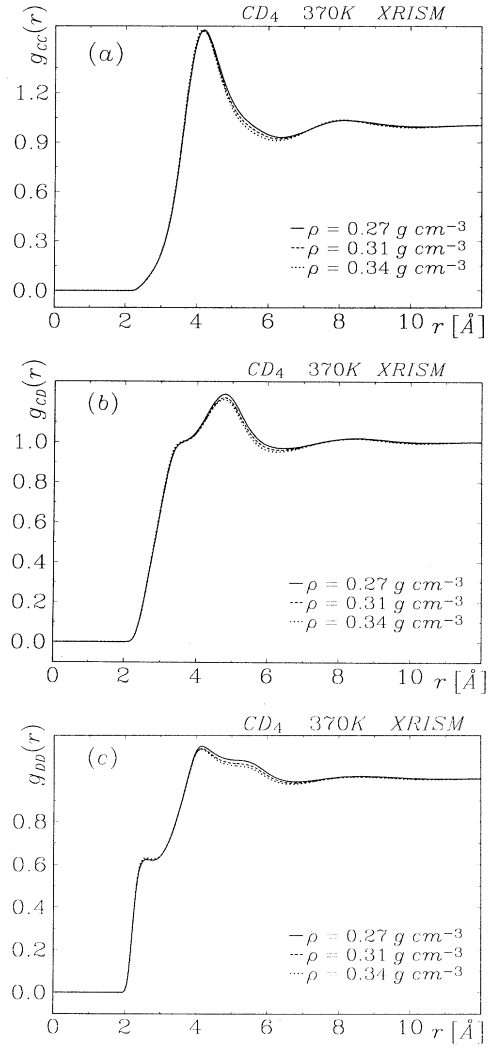

FIG. 7. (a)–(c) Atom pair correlation functions g_{CC}, g_{CD}, and g_{DD} (from top to bottom) of CD_4 at different thermodynamic states, calculated with XRISM theory (HNC closure).

TABLE VI. General reverse Monte Carlo simulation parameters of fluid CD_4: f_w, weighting factors of the atom pair correlation function; r_c, closest atom-atom distances for the initial configuration; r_g and σ_g, Gaussian maximum and the corresponding width.

	f_w	r_c (Å)	r_g (Å)	σ_g (Å)
C-C	0.039	3.2	3.400	0.200
C-D	0.320	2.4	2.600	0.200
D-D	0.641	2.2	2.400	0.075

percentual value for the reduce of the threshold value.

The other method we tested, the great deluge algorithm, is similar to TA but easier to realize. A new configuration is accepted if the χ^2 value is below the limit χ^2_{max}. After each acceptance, the value of the limit is reduced by a definite percentage, i.e., *gd%* of the difference between the current limit and the new χ^2 value. The algorithm leads to convergence within a sufficient number of simulation steps. So the GD algorithm depends only on two parameters: the initial value for χ^2_{max} and the decrease percentage *gd%*. From all that, it follows that the main difference between simulation runs based on the TA or the GD algorithm is the different treatment of χ^2_{max}, which continuously decreases in the case of the GD algorithm, whereas the TA rules admit increases of this upper limit.

We applied both modified RMC methods on the recently published total atom pair correlation functions of liquid SF_6 obtained by neutron scattering [57] and compared the results with those obtained using the Gaussian algorithm described above. It turned out that a considerably better agreement between the experimental and the calculated functions can be achieved with both new algorithms. Of course, when employing a new method, one has to realize its limits. In the case of RMC calculations we have to take into account that computer simulations that are not based on intermolecular potentials can generate a configuration that is not representative of the most probable one [61]. But without discussing this fundamental question of the RMC method itself, it is obvious that the employment of these new algorithms leads to an increase in the reliability of the fitting procedure results. Over the course of several tests of the GD algorithm it became apparent that the simulation run is largely independent of the initial value of χ^2_{max}, provided it is sufficiently greater than the initial value of χ^2. Therefore, only the single parameter *gd%* is necessary for the optimization, which makes this algorithm very easy to handle. As the efficiency of these two methods is similar (the TA algorithm is more complex and requires the optimization of three parameters), we referred the GD algorithm, but it should be noted that our preference for the GD method does not exclude the possibility that the TA algorithm is the more suitable choice in the case of other, e.g., nonspherical, systems.

B. Calculations and results

For all measured densities 20 simulation runs with the great deluge algorithm were performed and the resulting functions were averaged. Each run started from a different randomly generated initial configuration with 1000 molecules in the inner sphere and a shell of the thickness $R_{max}=16$ Å. The methane molecule has been treated as a regular tetrahedron with a C-D bonding length of 1.1 Å. Over the course of the simulation procedure random displacements and orientational changes up to the maximum values of 0.5 Å for the distance and 30° for the angles, respectively, per step were admitted. The closest atom-atom distances, defined by σ_g and r_g, are given in Table VI. For the calculation of the χ^2 value, only the distances up to a maximum value of 12 Å have been used in order to avoid any influence of termination-of-series effects, caused by the finite shell width. The experimental error has been assumed to be a constant value of 0.03 Å. The most important simulation parameters are summarized in Table VII.

After moving each particle 100 times convergence of the simulated total atom pair correlation function to the experimental one was reached with a very good fit parameter (see Table VII), even for the density with the worst χ^2 value ($\rho=0.27$ g/cm^3), as can be seen in the averaged function in Fig. 8. The averaged and slightly smoothed

TABLE VII. Reverse Monte Carlo simulation parameters and results for each simulation run: ρ, density; ρ_n, number density; N_i, number of molecules in the inner sphere; N_g, total number of molecules; R_i, radius of the inner sphere; R_{max}, thickness of the shell; χ^2_{max}, initial upper limit for the χ^2 value; *gd%*, decrease parameter for the χ^2 value.

ρ (g/cm^3)	0.27	0.31	0.34
ρ_n (Å^{-3})	0.008 36	0.009 19	0.010 21
N_i	1000	1000	1000
N_g	3536	3654	3793
R_i (Å)	30.5658	29.6164	28.5953
R_{max} (Å)	16	16	16
χ^2_{max}	10 000	10 000	10 000
gd%	1.1	0.8	1.0
steps per molecule	100	100	100
averaged configurations	20	20	20
average acceptance ratio (%)	61	63	55
average χ^2 value	0.1537	0.0630	0.0769

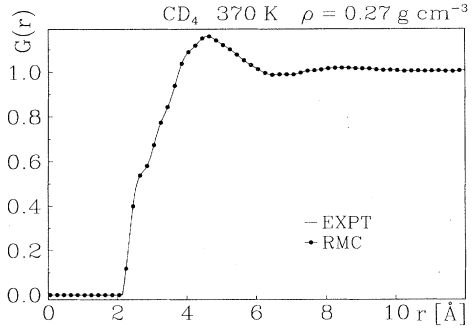

FIG. 8. Intermolecular total atom distribution functions of CD_4 at $T=370$ K and $\rho=0.27$ g cm^{-3}, for experimental results and RMC simulations.

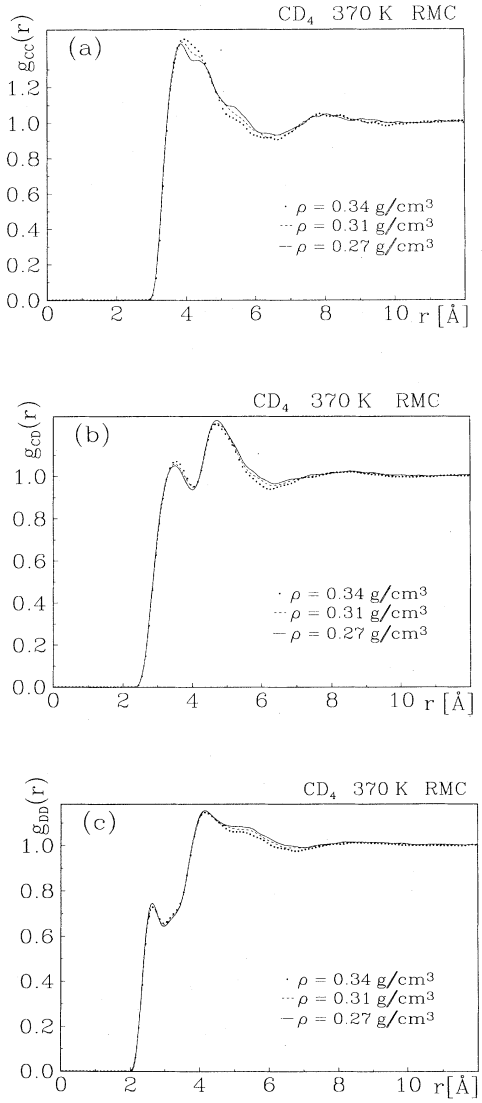

FIG. 9. (a)–(c) Atom pair correlation functions g_{CC}, g_{CD}, and g_{DD} of CD_4 at different thermodynamic states, calculated by RMC simulations.

atom pair correlation functions (see Fig. 9) show only small density effects, which are most significant in the C-C atom pair correlation function. The first maximum at 4.0 Å is reduced with decreasing density whereas the shoulder at 4.5 Å is more pronounced. The integration of the C-C correlation function up to 6.3 Å yields the total number of methane molecules in this radius as 10.2 for the highest and 8.5 for the lowest density. It is quite likely that this effect can be attributed to the decrease of the density values alone. The shape of the C-D and the D-D correlation functions indicates only very weak density effects as well.

C. Orientational correlations

Recognizing that the information derived from the pair correlation functions is not sufficient to describe the short-range order in a satisfactory manner, we calculated the angle distribution functions from the final configurations. First, we computed the angles of all center-center-center-triangles, taking into account all distances up to a value of d_{max}, which we chose as 6 and 12 Å. The resulting distribution functions were normalized to the theoretical functions of a completely disordered system with molecules treated as dots.

The averaged and slightly smoothed functions depicted in Fig. 10 show only one maximum at small angles (55° for $d_{max}=6$ Å and 30° for $d_{max}=12$ Å). This can be attributed to the minimum distances between the molecules, which prevent the occurrence of smaller angles if both sides are of the same length, and does not indicate any

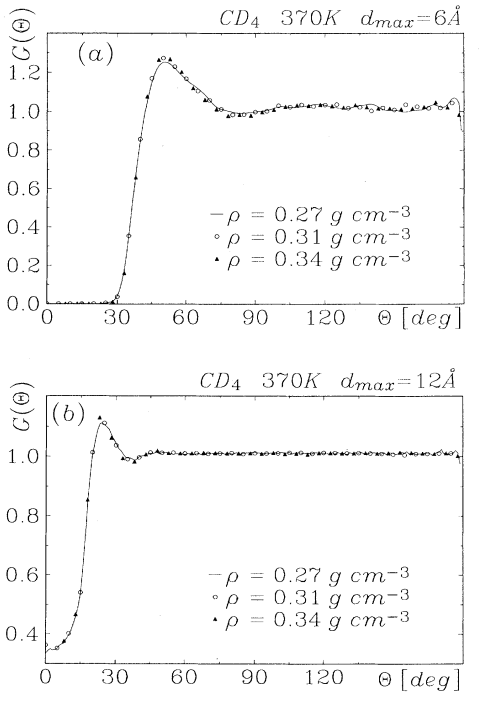

FIG. 10. Center-center-center angular distribution normalized to the shell surface, including center distances up to the upper limits (a) $d_{max}=6$ Å and (b) $d_{max}=12$ Å.

structural peculiarity. Apart from that, the angles are completely statistically distributed and there is no similarity to the angle distribution function expected for a fcc lattice, as occurs in the low-temperature phases of solid methane [62]. As the high-temperature phase is an orientationally disordered phase [6], it makes sense that our results indicate a completely statistical distribution of the molecule centers in the liquid. Furthermore, we determined the distribution of the angles between the C-D axes in steps of 30° depending on the center distance. In order to avoid effects due to the different intensities of the center-center correlation functions, the angular distribution functions were normalized to $g_{cc}(r)$. As shown in the slightly smoothed functions in Fig. 11, there are no predominating angles at any center distance. Therefore we can deduce that the methane molecules are completely orientationally disordered in the fluid phase with respect to both the distribution of the centers as well as to their relative orientation, at all measured densities.

VIII. CALCULATION OF THE MOLECULAR CENTER STRUCTURE FACTOR AND CONCLUSION

If the conclusion, based on the RMC calculations, is correct, namely, that no orientational correlation in the fluid phase exists, the Fourier transform of the center-center correlation function multiplied by the square of the molecule form factor should describe the experimentally determined intermolecular structure factor. We calculated the molecule form factor of methane according to

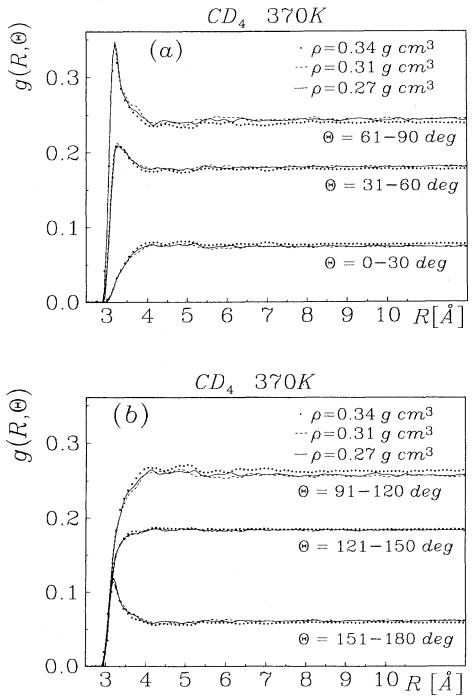

FIG. 11. Angular distribution functions of the angles between the C-D axes of the methane molecules, normalized to $g_{CC}(r)$, for all measured densities.

TABLE VIII. Parameters of the CC interaction of the potentials for the calculations of the molecular center structure factor of methane at the investigated temperature and densities. The parameters were taken from literature and deduced in this work.

ϵ (kJ mol^{-1})	σ (Å)	Reference
1.1973	3.79	[53]
1.1391	3.88	[53]
0.60	3.70	[11]
0.40	3.25	[52]
0.60	2.60	this work

Eq. (12) and tested the carbon-carbon correlation function obtained from XRISM calculations and from RMC simulations by comparing the results with the experiment. Additionally, we calculated the center-center correlation function with XRISM, using the potential parameters found in literature, and compared the results with the experiment. The parameters used are given in Table VIII. An example for one measured density is shown in Fig. 12. Although the carbon-carbon correlation function contributes only 4% to the total atom pair correlation function of methane and the density effects are rather small, the RMC results and the CC atom pair correlation function, calculated with the potential deduced in this work, fit the experiment in an astonishingly good manner at all investigated thermodynamic states, as can be seen in Fig. 12 for one density. The misfit in the large-κ region is caused by neglecting higher-order terms in the approximation and is visible in all results of the calculated potentials.

It can be concluded, which is important for further investigations, that the CD_4 molecule can be assumed as being spherical and that at the determined thermodynamic conditions the molecules in fluid CD_4 are statistically

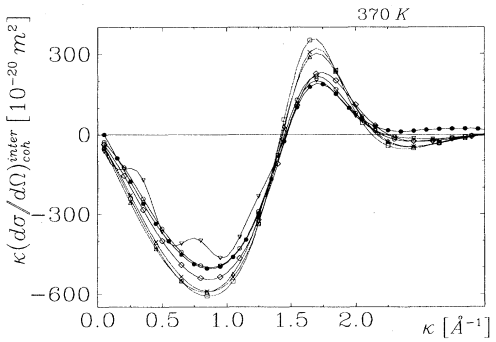

FIG. 12. Intermolecular part of the experimental differential scattering cross section of CD_4 and theoretically calculated molecular center structure factors at $T=370$ K and density $\rho=0.34$ g cm^{-3}. ● denotes experiment. The other curves with symbols are the results of statistical mechanical calculations, based on potentials deduced in this work or found in literature (the parameters are given in Table VIII): △, [52]; ◇, [53]; □, [53]; ×, [11]; ○, this work (XRISM); ▽, this work (RMC).

distributed with completely disordered molecule axes and that density effects are only quite weak. Therefore our results support the statement of Habenschuss, Johnson, and Narten [23] that apart from the nearest-neighbor interactions the structure has very great similarity to that of a nonassociated atomic fluid.

ACKNOWLEDGMENTS

The authors gratefully acknowledge the BMFT for financial support (Contract No. 03-BE3STU). We also wish to thank R. Aich for the technical assistance.

[1] I. Prigogine, A. Bellemans, and V. Mathot, *The Molecular Theory of Solutions* (North-Holland, Amsterdam, 1957).
[2] T. Boublik and F. Nezbeda, Colln. Czech. Chem. Commun. **51**, 2301 (1986).
[3] A. L. Archer and G. Jackson, Mol. Phys. **73**, 881 (1991).
[4] D. J. Tildesley, E. Enciso, and P. Sevilla, Chem. Phys. Lett. **100**, 508 (1983).
[5] D. Chandler, Annu. Rev. Phys. Chem. **29**, 441 (1978).
[6] J. S. Rowlinson and F. L. Swinton, *Liquids and Liquid Mixtures* (Butterworths, London, 1982).
[7] L. Lue and D. Blankschtein, J. Phys. Chem. **96**, 8582 (1992).
[8] D. P. Shelton, G. C. Tabisz, F. Barocchi, and M. Zoppi, Mol. Phys. **46**, 21 (1982).
[9] A. Tani, Chem. Phys. Lett. **105**, 72 (1984).
[10] B. Plenkiewicz, P. Plenkiewicz, J. P. Jay-Gerin, and K. Jain, J. Chem. Phys. **90**, 4907 (1989).
[11] S. K. Datta, Indian J. Pure Appl. Phys. **21**, 280 (1983).
[12] U. Bafile, L. Ulivi, M. Zoppi, F. Barocchi, and L. Frommhold, Phys. Rev. A **50**, 1172 (1994).
[13] R. Righini, K. Maki, and M. L. Klein, Chem. Phys. Lett. **80**, 301 (1981).
[14] S. Murad, K. E. Gubbins, and J. G. Powles, Mol. Phys. **40**, 253 (1980).
[15] G. P. Matthews and E. B. Smith, Mol. Phys. **32**, 1719 (1976).
[16] M. K. Kansal and S. K. Trikha, Aust. J. Phys. **46**, 523 (1993).
[17] R. H. Kincaid and H. A. Scheraga, J. Phys. Chem. **86**, 833 (1982).
[18] V. V. Sychev, A. A. Vasserman, V. A. Zagoruchenko, A. D. Kozlov, G. A. Spiridonov, and V. A. Tsymarny, *Thermodynamic Properties of Methane* (Springer-Verlag, Berlin, 1987).
[19] T. Johnson and L. G. Olsson, Physica B **115**, 15 (1982).
[20] T. Johnson and L. G. Olsson, Physica B **122**, 227 (1983).
[21] N. Meinander and G. C. Tabisz, J. Chem. Phys. **79**, 416 (1983).
[22] G. C. Tabisz, Chem. Phys. Lett. **52**, 125 (1977).
[23] A. Habenschuss, E. Johnson, and A. H. Narten, J. Chem. Phys. **74**, 5234 (1981).
[24] P. Chieux, *Neutron Diffraction,* edited by Hrsg. H. Dachs, Topics in Current Physics Vol. X (Springer-Verlag, Berlin, 1978).
[25] C. Windsor, *Pulsed Neutron Scattering* (Academic, London, 1981).
[26] P. A. Egelstaff, in *Neutron Scattering,* edited by K. Sköld and D. L. Price (Academic, London, 1987), Vol. 23.
[27] P. Chieux, J. Mol. Struct. **296**, 177 (1993).
[28] M. L. Boas, *Mathematical Methods in Physical Sciences* (Wiley, New York, 1983).
[29] R. W. James, Phys. Z. **33**, 737 (1932).
[30] H. Menke, Phys. Z. **33**, 593 (1932).
[31] Hrsg. I. L. Spain and J. Paauwe, *High Pressure Technology* (Dekker, New York, 1977).
[32] T. Bausenwein, H. Bertagnolli, K. Tödheide, and P. Chieux, Ber. Bunsenges. Phys. Chem. **95**, 577 (1991).
[33] Science and Engineering Research Council, User Guide, Experimental Facilities at ISIS, Rutherford Appleton Laboratory, Chilton, Didcot, Oxon OX11 OQX, United Kingdom, 1990.
[34] A. K. Soper, W. S. Howells, and A. C. Hannon, *Analysis of Time-of-Flight Diffraction Data from Liquid and Amorphous Samples* (Rutherford Appleton Laboratory, Chilton, 1989).
[35] A. K. Soper and P. A. Egelstaff, Nucl. Instrum. Methods **178**, 415 (1980).
[36] G. Placzek, Phys. Rev. **86**, 377 (1952).
[37] J. G. Powles, Mol. Phys. **26**, 1325 (1976).
[38] J. G. Powles and G. Rickayzen, Mol. Phys. **32**, 301 (1976).
[39] J. G. Powles and G. Rickayzen, Mol. Phys. **32**, 323 (1976).
[40] J. G. Powles, Mol. Phys. **36**, 1161 (1978).
[41] J. G. Powles, Mol. Phys. **36**, 1181 (1978).
[42] J. G. Powles, Mol. Phys. **37**, 623 (1979).
[43] J. U. Weidner, H. Geisenfelder, and H. Zimmermann, Ber. Bunsenges. Phys. Chem. **75**, 800 (1971).
[44] W. H. Press, B. P. Flannery, S. A. Teukolsky, and W. T. Vetterling, *Numerical Recipes* (Cambridge University Press, Cambridge, 1990).
[45] F. Hirata and P. J. Rossky, Chem. Phys. Lett. **83**, 329 (1981).
[46] F. Hirata, B. M. Pettitt, and P. J. Rossky, J. Chem. Phys. **77**, 509 (1982).
[47] B. M. Pettitt and P. J. Rossky, J. Chem. Phys. **77**, 1451 (1982).
[48] B. M. Pettitt and P. J. Rossky, J. Chem. Phys. **78**, 7296 (1983).
[49] E. Bartsch and H. Bertagnolli, Ber. Bunsenges. Phys. Chem. **91**, 745 (1987).
[50] J. K. Percus and G. J. Yevick, Phys. Rev. **110**, 1 (1958).
[51] G. S. Rushbrooke and H. I. Scoins, Proc. R. Soc. London Ser. A **216**, 203 (1953).
[52] D. E. Williams, J. Chem. Phys. **47**, 4680 (1967).
[53] J. O. Hirschfelder, C. F. Curtiss, R. B. Bird, *Molecular Theory of Gases and Liquids* (Wiley, New York, 1964).
[54] R. L. McGreevy and L. Pusztai, Mol. Sim. **1**, 359 (1988).
[55] M. Ostheimer and H. Bertagnolli, Z. Phys. Chem. **162**, 171 (1989).
[56] H. Bertagnolli, H. Zweier, and A. David, Ber. Bunsenges. Phys. Chem. **97**, 1125 (1993).
[57] G. Strauβ, H. Zweier, H. Bertagnolli, T. Bausenwein, K. Tödheide, and P. Chieux, J. Chem. Phys. **101**, 662 (1994).
[58] G. Dueck and T. Scheuer, J. Comput. Phys. **90**, 161 (1990).
[59] G. Dueck, T. Scheuer, and H.-M. Wallmeier, Spektrum

Wissenschaft. **3**, 42 (1993).
[60] G. Dueck, J. Comput. Phys. **104**, 86 (1993).
[61] T. Radnai, I. Bako, and P. Jedlovszky, Mol. Phys. **83**, 459 (1994).
[62] S. Greer and L. Meyer, J. Chem. Phys. **52**, 468 (1970).
[63] R. A. Olafson, M. A. Thomas, and H. L. Welsh, Can. J. Phys. **39**, 436 (1961).
[64] G. G. Shepherd and H. L. Welsh, J. Mol. Spectrosc. **1**, 286 (1957).
[65] L. S. Bartell and K. Kuchitsu, J. Chem. Phys. **35**, 1211 (1961).
[66] V. W. Laurie and D. R. Hersbach, J. Chem. Phys. **37**, 1687 (1962).